Journal of Alloys and Compounds 509 (2011) 4696–4700

Contents lists available at ScienceDirect

Journal of Alloys and Compounds

journal homepage: www.elsevier.com/locate/jallcom

On the chloride-induced pitting of ultra fine grains 5052 aluminum alloy produced by accumulative roll bonding process

Mehdi Fadaei Naeini*, Mohammad Hossain Shariat, Mehdi Eizadjou

Department of Materials Science & Engineering, Shiraz University, Shiraz, Iran

ARTICLE INFO

Article history:
Received 17 October 2010
Received in revised form 5 January 2011
Accepted 8 January 2011
Available online 15 January 2011

Keywords:
AA 5052
Pitting corrosion
Accumulative roll-bonding

ABSTRACT

Pitting corrosion susceptibility of ultra fine grain (UFG) 5052 aluminum alloy (AA 5052) sheets highly deformed by accumulative roll-bonding (ARB) was investigated in 3.5 wt% NaCl solution using potentiodynamic polarization, cyclic voltammetry and immersion tests. The morphology of localized attacks was analyzed by SEM-EDS. Pitting corrosion resistance of samples was diminished with increasing the number of ARB passes which is presumably due to microstructure refinement and increasing the defect density.

1. Introduction

Several severe plastic deformation (SPD) processing techniques such as equal-channel angular pressing (ECAP) [1], high-pressure torsion (HPT) [2], multi-axial compressions/forging (MAC/F) [3] and accumulative roll-bonding (ARB) [4,5] were developed in the past two decades to obtain UFG structures in both bulk and sheet materials. The ARB process is a relatively novel method proposed by Saito et al. [4] in order to fabricate a submicron/nanograin structure in various kinds of sheet materials. In the ARB process, an extremely high plastic strain was imposed on the materials which results in structural refinement and increasing the strength without changing specimen dimensions [4]. Microstructure and mechanical properties of aluminum and its alloys subjected to ARB process had been extensively investigated [5–10]. However, apparently little is known about the corrosion behavior of UFG Al-alloys fabricated by ARB process. A number of studies [11–13] have found that SPD processes can either increase or decrease corrosion resistance of various aluminum alloys. It seems that corrosion resistance of such UFG materials mainly depends on chemical composition of alloy and corrosive media as well as the type of SPD process. Wei et al. [12] have reported that the corrosion resistance of UFG Al–Mn alloy fabricated by ARB process in 3.5% NaCl artificial seawater was improved due to decreasing in size of $MnAl_6$ particles. In another study, corrosion behavior of three different ECAP-processed Al-alloys in natural buffer solution containing 0.002 M NaCl evaluated by Akiyama et al. [13]. They pointed out that pitting corrosion resistance of ECAP processed pure aluminum was deteriorated because of generated dislocations and grain boundaries. Whereas two other Al alloys containing 5.4 wt% Ni and 5 wt% Cu, respectively, exhibited improved pitting corrosion resistance than their coarse grain (CG) counterparts. These variations were explained in terms of α-Al crystals refining and decreasing of Cu depleted regions where preferential initiation of pits take place.

Sheets of 5*xxx*-series aluminum alloys have been widely used in industry due to their high strength to density ratio, good formability, good weldability and high levels of corrosion resistance [14]. So it should be interesting to determine how ARB process can affect the pitting corrosion behavior of these alloys. To achieve this goal, chloride-induced pitting of ARB-processed AA 5052 sheets was investigated.

2. Experimental procedure

2.1. Specimen preparation by means of ARB process

5052 aluminum alloy sheets with the chemical composition given in Table 1 were used in this study. Fully annealed sheets of 300 mm long, 30 mm wide, and 1 mm thick were prepared with consistent specimen hardness and equiaxed grains with the mean grain size of 30 μm.

In the ARB process, the sheets were wire-brushed (circular steel brush with 0.35 mm diameter wire and surface speed of ~13.5 m/s) to remove surface oxides and, then degreased with acetone. Fig. 1 illustrates the principle of ARB process. Two sheets were stacked and bound tightly. Then the stacked sheets were rolled to 50% reduction in thickness. The roll-bonded sheet was cut in half and stacked to the initial thickness. The stacked sheets were rolled again with the same reduction ratio and the same procedure was repeated up to five cycles (the total equivalebt strain was 4) at ambient temperature. Roll bonding was carried out without any lubricant by the use of two mills having a roll diameter of 136 mm. The roll peripheral speed was 2.35 m/min, so that the mean strain rate during the roll-bonding

* Corresponding author. Tel.: +98 912 6222293.
E-mail address: Fadaei.9i@gmail.com (M.F. Naeini).

0925-8388/$ – see front matter © 2011 Elsevier B.V. All rights reserved.
doi:10.1016/j.jallcom.2011.01.066

Table 1
Chemical composition of 5052 aluminum alloy.

Alloying elements	Mg	Fe	Cr	Si	Ti	Mn	Cu	Zn	Ni	Al
wt.%	2.48	0.26	0.18	0.085	0.028	0.008	0.004	0.004	0.002	Base

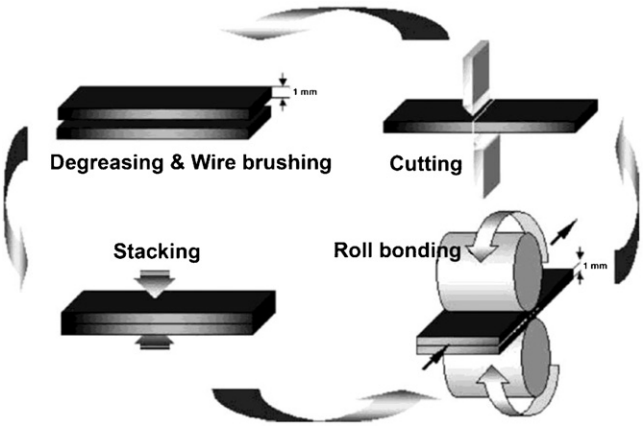

Fig. 1. Schematic illustration of the principle of ARB process [9].

was 4.55 s^{-1}. The sheets were cooled in air after roll-bonding process. Transmission electron microscope (TEM) microstructure of the 5 passes ARB-processed specimen was observed by the use of a Philips FEG transmission electron microscope operated at 200 kV. Thin foils parallel to the rolling plane were prepared by means of twin-jet electropolishing in a 400 ml HNO_3 and 800 ml CH_3OH solution at the temperature of 253 K.

2.2. Electrochemical assessments and surface observations

In all electrochemical experiments and immersion tests, aqueous solutions of sodium chloride (distilled water and reagent grade NaCl) with concentration of 3.5 wt% NaCl were used as the corrosive medium. The working electrodes made from ARB-processed sheets of AA 5052, machined into 11.3 mm diameters disk shape and mounted into acrylic resin. This produced a 1 cm^2 one-dimensional circular surface of electrode exposed to the corrosion medium. Each disk shape sample was mechanically polished successively with SiC abrasive paper up to 2000 grade, washed with distilled water, degreased with ethanol and introduced into distilled water. Experiments were conducted in a single compartment three-electrode cell of 400 ml volume. All potentials measured against an Ag/AgCl (3 M KCl) reference electrode and platinum rod was used as the counter electrode. Electrochemical experiments were carried out with a μAUTOLAB type III electrochemical system. The experimental data were acquired and processed with the GPES 4.9.006 computer program.

After each pass of ARB process, determination of open circuit potential (OCP) was carried out after 12 h immersion in NaCl solution, and then, potentiodynamic polarization and cyclic voltammetry tests were performed at a scan rate of 0.5 mV/s. In the case of cyclic voltammetry, the potential sweep was reversed at current density of 10 mA/cm^2. A clockwise hysteresis loop is traced during reverse scan, indicating the possibility of pitting in susceptible alloy. Two pitting parameters, namely the critical pitting potential (E_{pit}), and the protection potential (E_{prot}) can be determined from these tests. The value of E_{pit} denotes the potential at which current increases abruptly on the forward scan indicating the possibility of pit initiation. E_{prot} indicates the electrochemical potential at which the current returns to passive values during reverse scan, indicating repassivation of pits.

The surface morphology and elemental analysis of samples after three weeks immersion in corrosive medium were investigated using a Cambridge Stereo Scan SEM-EDS system.

3. Results

3.1. TEM microstructure

Fig. 2 shows TEM micrographs and corresponding selected area electron diffraction (SAD) pattern of AA5052 after 5 passes of accumulative roll bonding at room temperature. It seems that the specimen was filled with the ultra-fine grains in which the dislocation density is very low inside, and are surrounded by clearly and strongly deformed boundaries (high angle grain boundaries), which have a high density of dislocations. Rings and diffused spots from SAD pattern of the 5 passes sample indicate the large misorientation exists between grains as well as high angle grain boundaries. TEM observation (Fig. 2) illustrates AA5052 ARB-processed sample up to 5 passes was covered with the ultra-fine grains between 100 and 300 nm in average diameter, homogenously distributed.

3.2. Electrochemical experiments

Fig. 3 shows anodic potentiodynamic polarization curves of annealed and ARB-processed AA5052 in 3.5 wt% NaCl solution. In the case of annealed sample, during the positive potential sweep from corrosion potential ($E_{corr} \approx -0.7$ V), alloy exhibits passive behavior which is typical of aluminum alloys. It is well known that a thin oxide film of basically Al_2O_3 is immediately formed on the aluminum alloys upon its exposure to air or moisture [15,16]. An anodic current appears at −0.575 V which indicates a breakdown potential (E_{bd}) at which destruction of passive film begins. Proceeding of ARB process for 3 and 5 passes decreases E_{bd} values to −0.585 V and −0.645 V, respectively (Fig. 3).

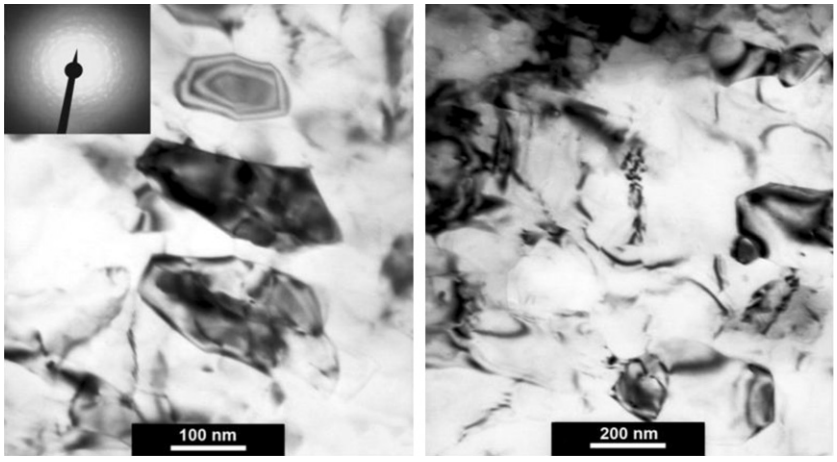

Fig. 2. TEM micrographs and corresponding SAD pattern of AA 5052 specimen ARBed by 5 passes.

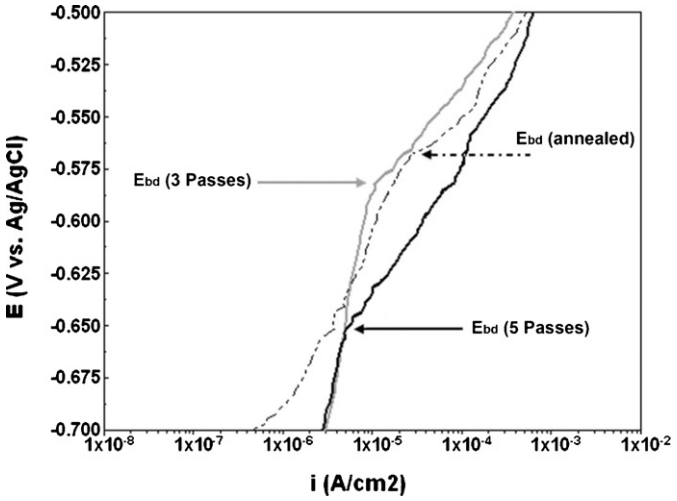

Fig. 3. Anodic potentiodynamic polarization curves of annealed, 3 passes, and 5 passes ARB-processed samples in 3.5 wt% NaCl solution.

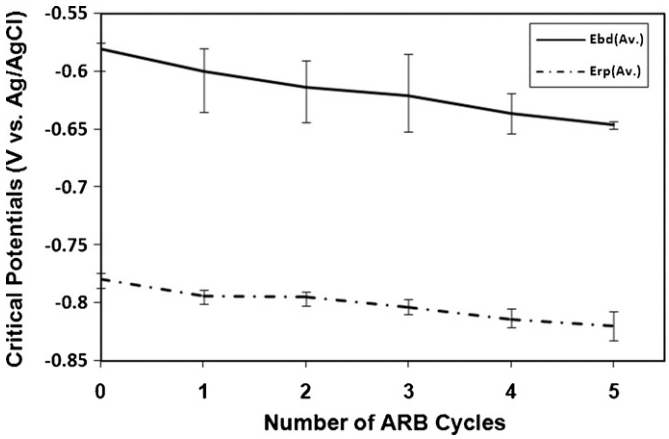

Fig. 5. Effect of ARB process on the breakdown and repassivation potentials of 5052 aluminum alloy in 3.5 wt% NaCl solution.

Cyclic voltammetry behavior of annealed and ARB-processed alloy samples in 3.5 wt% NaCl solution are shown in Fig. 4. A reverse potential sweep in negative direction leads to formation of a hysteresis loop which implies that localized corrosion is taking place at alloy surface [17]. Potential at which the current density reaches to passive current density is called repassivation potential (E_{rp}). As it can be seen, processing of 3 and 5 passes ARB causes E_{rp} shifted 33 and 55 mV, respectively, toward lower values. Both E_{bd} and E_{rp} values may serve as certain criteria of an anticorrosive stability: the higher the potential the more stable the metal [17]. Critical pitting potentials (E_{bd} and E_{rp}) of alloy samples as a function of ARB passes obtained from electrochemical experiments are exhibited graphically in Fig. 5. These potentials decrease slightly with increasing the number of ARB passes. Therefore, it is understood that pitting corrosion resistance of alloy will be diminished in each step of ARB passes.

3.3. Immersion tests

Fig. 6 shows SEM micrographs of annealed and ARB-processed sample surfaces after three weeks immersion in 3.5 wt% NaCl solution. Localized corrosion damage in the all samples is obvious and severity of pitting attacks is enhanced by ARB process. As can be

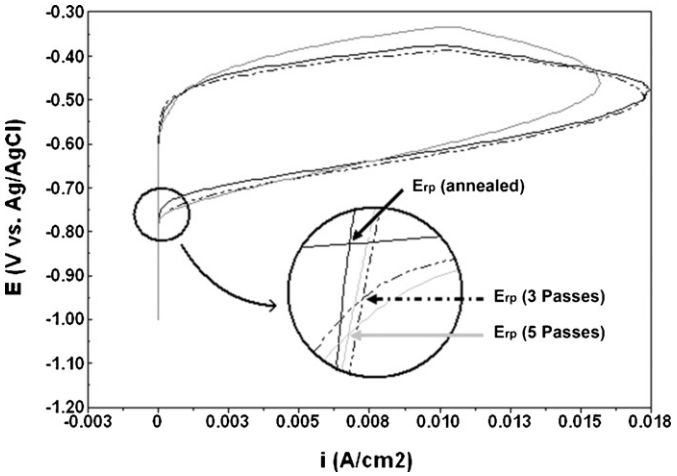

Fig. 4. Cyclic voltammograms for annealed, 3 passes, and 5 passes ARB-processed samples in 3.5 wt% NaCl solution.

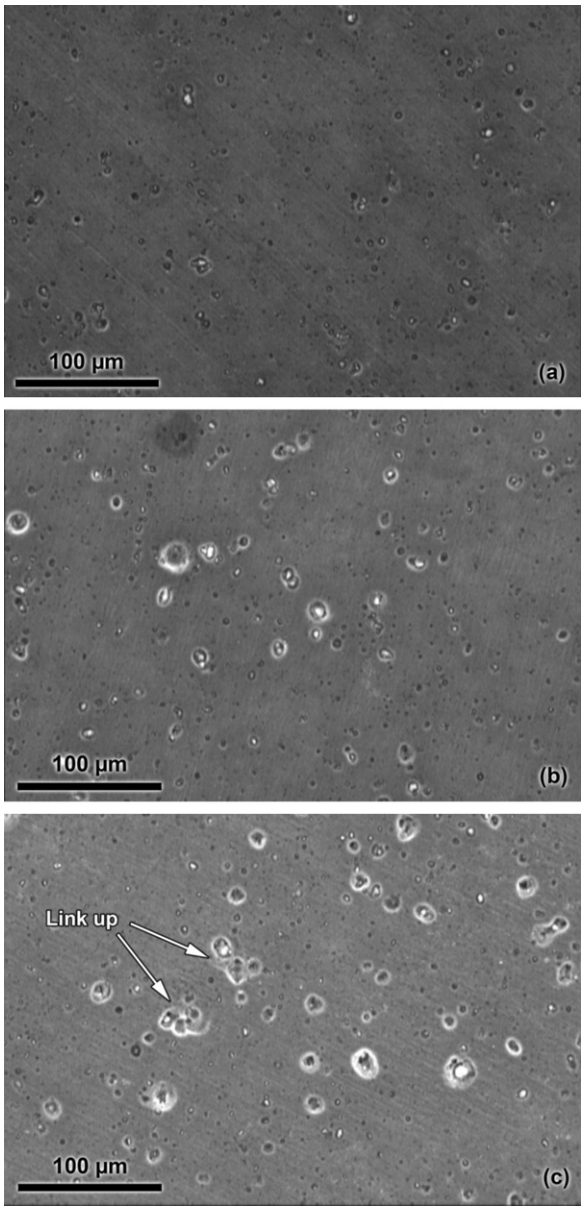

Fig. 6. SEM micrographs of (a) annealed, (b) 3 passes, and (c) 5 passes ARB-processed sample surfaces after three weeks immersion in 3.5 wt% NaCl solution.

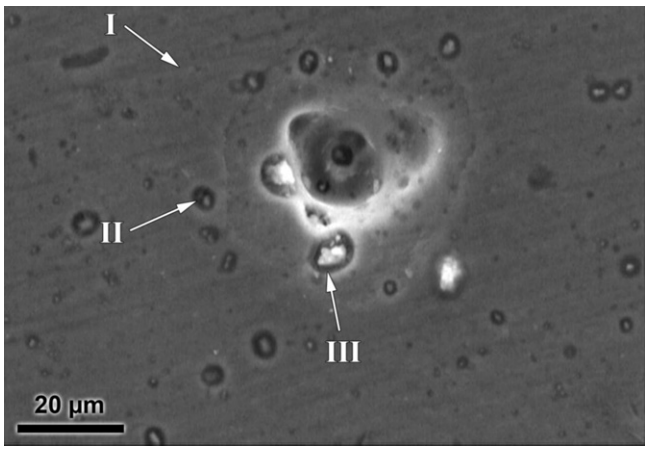

Fig. 7. SEM image of 2 passes ARB-processed sample surface after immersion in 3.5 wt% NaCl solution.

seen in Fig. 6a, there are relatively small and shallow pits with symmetrical geometry distributed uniformly over the surface of annealed sample. Proceeding of ARB process for 3 (Fig. 6b) and 5 (Fig. 6c) passes produces a mixture of very small pits accompanied by irregular larger and deeper ones. Such morphology is more evident in the sample which underwent 5 ARB passes. As it was illustrated in the Fig. 6c, adjacent smaller pits can link up to form larger pits.

SEM micrograph of 2 passes ARB-processed sample surface after immersion test was shown in Fig. 7. Different regions of Fig. 7 were analyzed by EDS analysis(Figs. 8a–c) in order to investigate the type of existing intermetallics in these locations. Fig. 8a represent EDS analysis corresponding to region I (Fig. 7) which include just aluminum peak and indicates α-Al matrix. Two types of initiation site for pitting attacks are visible in Fig. 7, the darker sites include region II which contain Fe (Fig. 8b) and the brighter sites include region III which contain Mg (Fig. 8c). These results demonstrate that initiation of pitting corrosion can occur either at iron rich and magnesium rich intermetallic compounds.

4. Discussion

A vast number of papers [18–28] have been published through the years on the factors affecting pitting corrosion susceptibility of aluminum alloys in halide salt solutions. It is definitely dependent upon the alloy composition, presence and distribution of micro-defects (e.g., vacancies, voids, and etc.), as well as macro-defects (e.g., second phase particles, inclusions, and etc.), and crystal structure of the oxide film [18]. As stated by point defect model [29] for the pitting corrosion of aluminum alloys, chloride ions adsorb, and then, incorporate to the oxide film by occupying anion vacancies. In contrast with anion vacancies, the number of cation vacancies increase and start to accumulate at the metal/oxide interface. As a result, passive film is broken down and pitting will be commenced. Deferent analytical techniques such as autoradiography [30], Secondary ion mass spectroscopy (SIMS) [31], and X-ray photoelectron spectroscopy (XPS) [32,33] exhibited local adsorption of Cl^- ions on the defects and inhomogeneities of aluminum oxide films because of lower adsorption energy in these sites. It is deduced that a less defective oxide film with lower localized states, is more resistant to pitting corrosion [18].

Depending upon the alloying elements in various aluminum alloys, there are different types of intermetallic particles in the microstructure [16]. Due to galvanic interaction with the surrounding matrix constituent particles are well known sites for pit initiation [18,34–37]. Depending on initial composition, some constituent particles are cathodic to the matrix, and others are anodic [34]. Size, shape and distribution of intermetallic particles as a second phase influence the pitting corrosion behavior [38]. For example, it was found that the adsorption of Cl^- in passive film prefers at or around inclusions and second phase particles due to weaker oxide film on these sites [39]. 5*xxx* series of aluminum alloys contain mainly two types of intermetallics: Mg-rich particles which are anodic with respect to α-Al matrix and cathodic phases which primarily consist of Fe constituent [16,40]. The preferential initiation of localized corrosion attacks can be taken place at the both anodic phase/matrix and cathodic phase/matrix interfaces where local galvanic cells are formed (Fig. 7).

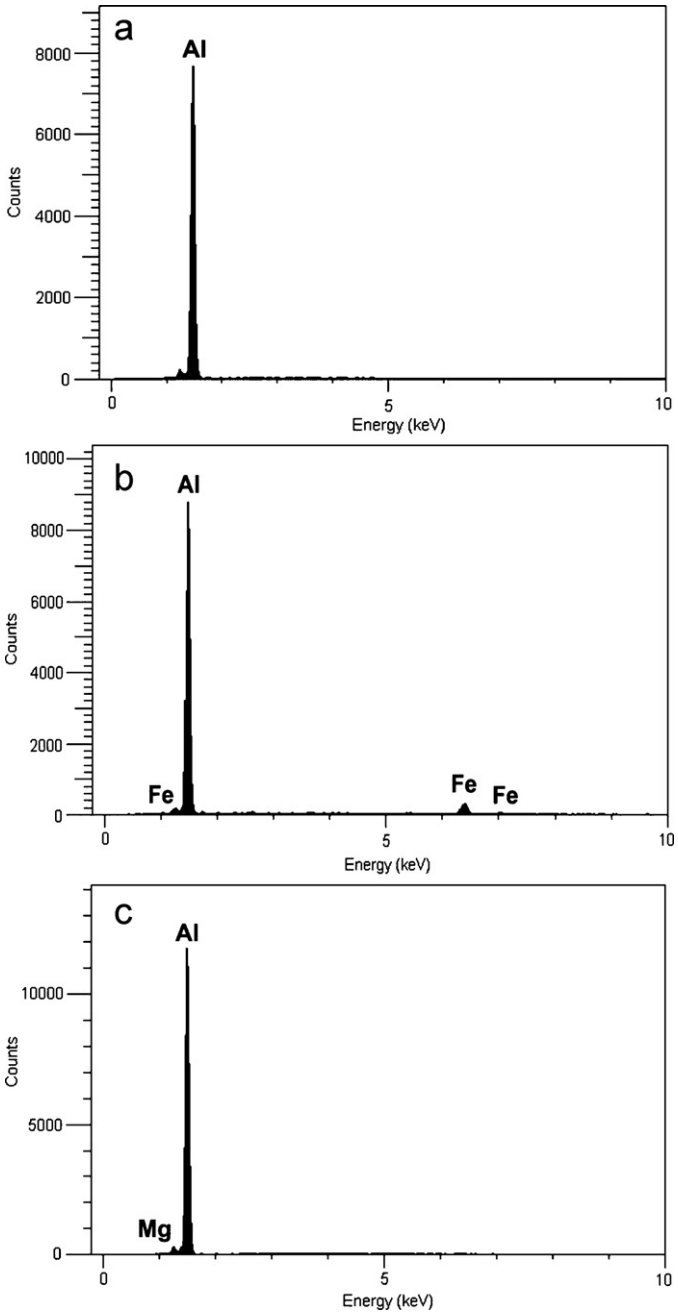

Fig. 8. EDS elemental analysis of regions (a) I, (b) II, and (c) III of Fig. 7.

Accumulative roll-bonding (ARB) process [4–10] was proposed to develop ultra-fine grained structures by introducing severe plastic strain in materials. As the process is progressed, subgrains (or dislocation cell structures) with high dislocation densities is formed

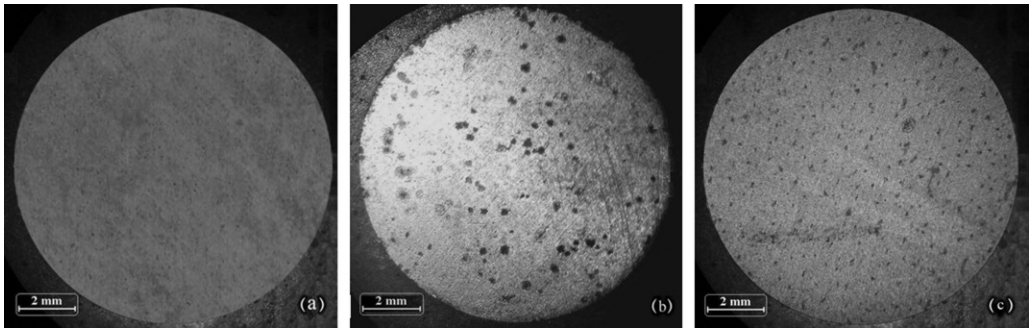

Fig. 9. Optical Stereoscan micrographs of (a) annealed, (b) 3 passes, and (c) 5 passes ARB-processed sample surfaces after three weeks immersion in 3.5 wt% NaCl solution.

and low-angle subgrain boundaries converted to high-angle grain boundaries. Fig. 2 showed formation of ultra-fine grains which are surrounded by sharp and strongly deformed low/high angle boundaries after proceeding of ARB process up to 5 passes. The oxide films which form on such high level energy and defectful substrate seem to have more defective structure. It is also noteworthy that as the number of ARB passes increase, intermetallic particles are refined [12], and thus, their total surface area is increased. Therefore, the preferential sites for initiation of localized corrosion, i.e. intermetallic/matrix interfaces, are increased (Fig. 9). The results obtained from electrochemical experiments (Fig. 5) and immersion tests (Fig. 6) demonstrated that pitting corrosion resistance of 5052 aluminum alloy is deteriorated under influence of ARB process, mainly due to the formation of more defective oxide layer as well as refinement of grains and second phase particles.

Moreover, it is clearly seen in Fig. 6 that intensity of pitting attacks is more rigorous in the samples which were undergone ARB process. The severity of pitting is dependent upon the degree of clustering of the particles [37]. A region of isolated particles will promote a mild shallow pitting attack. In a region with smaller clustered particles which can formed at higher ARB passes, the smaller pits can link up to form larger pits. This clustering can be across the surface, or it can be subsurface, which would promote deeper pitting [34,37].

5. Conclusion

Ultra fine grain microstructures with average grain size between 100 and 300 nm were formed in the 5052 aluminum alloy highly deformed by the ARB process. Effect of ARB process on the pitting corrosion behavior of aluminum alloy in 3.5 wt% NaCl solution was investigated by means of electrochemical experiments and SEM observations from immersed specimen surfaces. Pitting corrosion resistance of alloy was deteriorated due to the ARB process. It indicates that the formation of passive film is difficult with increase the cold deformations. This could be due to the enhanced dislocation density and defects [41]. The variations were explained through the formation of more defective, i.e., less protective oxide film originated from grain refinement and higher defect density in the bulk material. The severity of localized corrosion attacks was enhanced by the Clustered intermetallic particles in the final passes of ARB process.

Acknowledgment

This study supported by the Department of Materials Science and Engineering, Shiraz University. Special thanks are expressed to Ms. S. Monsef, Mrs. M. Paydar and Mr. E. Dehghanian for their help in performing this work.

References

[1] R.Z. Valiev, T.G. Langdon, Prog. Mater. Sci. 51 (2006) 881.
[2] R.Z. Valiev, R.K. Islamgaliev, I.V. Alexandrov, Prog. Mater. Sci. 45 (2000) 103.
[3] A.K. Gosh, U.S. Patent No. 4,721,537 (1998).
[4] Y. Saito, H. Utsunomiya, N. Tsuji, T. Sakai, Acta Mater. 47 (1999) 579.
[5] M. Eizadjou, H. Danesh Manesh, K. Janghorban, J. Alloys Compd. 474 (2009) 406.
[6] B.L. Li, N. Tsuji, N. Kamikawa, Mater. Sci. Eng. A 423 (2006) 331.
[7] M. Karlík, P. Homola, M. Slámová, J. Alloys Compd. 378 (2004) 322.
[8] H.W. Kim, S.B. Kang, N. Tsuji, Y. Minamino, Metall. Mater. Trans. A 36 (2005) 3151.
[9] B.K. Min, H.W. Kim, S.B. Kang, J. Mater. Process. Technol. 355 (2005) 162–163.
[10] S.H. Lee, Y. Saito, N. Tsuji, H. Utsunomiya, T. Sakai, Scripta Mater. 46 (2002) 281.
[11] M.K. Chung, Y.S. Choi, J.G. Kim, Y.M. Kim, J.Ch. Lee, Mater. Sci. Eng. A 366 (2004) 282.
[12] W. Wei, K.X. Wei, Q.B. Du, Mater. Sci. Eng. A 536 (2007) 454–455.
[13] E. Akiyama, Z. Zhang, Y. Watanabe, K. Tsuzaki, J.Solid State Electrochem. 13 (2009) 277.
[14] Y.M. Zhao, W.C. Liu, J.G. Morris, Metall. Mater. Trans. A 35 (2004) 3613.
[15] C. Vargel, Corrosion of Aluminum, Elsevier Press, Amsterdam, 2004.
[16] E.H. Hollingsworth, H.Y. Hunsicker, Metals Handbook, 13, 5th ed., ASM International, 1990.
[17] A. Ručinskienė, G. Bilkulčius, L. Gudavičiūtė, E. Juzeliūnas, Electrochem. Commun. 4 (2002) 86.
[18] Z. Szklarska-Smialowska, Corros. Sci. 41 (1999) 1743.
[19] H. Kaesche, Die Korrosion der Metalle: Physicalish-Chemishe Prinzipien und Acmelle Probleme, Springer, Berlin-Heidelberg, New York, 1979.
[20] S.S. Abdel Rehim, H.H. Hassan, M.A. Amin, Corros. Sci. 46 (2004) 921.
[21] K.V. Idem, The Electrochemistry of Uniform Corrosion and Pitting of Aluminium. Kjeller Report 62, Institute for Atommenergi, Kjeller, Norway, 1974.
[22] H.J.M. Lenderink, M.V.D. Linden, J.H.W. de Wit, Elecctrochim. Acta 38 (1993) 1989.
[23] C.M.A. Brett, J. Appl. Electrochem. 20 (1990) 1000.
[24] J.D. Lim, S.I. Pyun, Elecctrochim. Acta 40 (1995) 1863.
[25] A. Kolics, J.C. Polkinghorne, A. Wieckowski, Elecctrochim. Acta 43 (1998) 2605.
[26] K.H. Na, S.I. Pyun, H.P. Kim, Corros. Sci. 49 (2007) 220.
[27] G.E. Kiourtsidis, S.M. Skohanos, Corros. Sci. 49 (2007) 2711.
[28] K.N. Na, S.I. Pyun, Corros. Sci. 50 (2008) 248.
[29] C.Y. Chao, L.F. Lin, D.D. MacDonald, J. Electrochem. Soc. 128 (1981) 1187.
[30] A. Berzins, R.T. Lowson, K.J. Mirans, Aust. J. Chem. 30 (1977) 1891.
[31] G.C. Wood, J.A. Richardson, M.F. Rabbo, L.M. Mapa, W.H. Sutton, Passivity of Metals, Proceedings of the Fourth International Symposium on Passivity, The Electrochem. Soc., Pennington, NJ, 1978, p. 973.
[32] J. Augustynski, R.P. Frankenthal, Proceedings of the Fourth International Symposium on Passivity, The Electrochem. Soc., Pennington, NJ, 1978, p. 997.
[33] C. Blanc, G. Mankowski, Corros. Sci. 39 (1997) 949.
[34] J. Moran, Metals Handbook, 13A, ASM International, 2003, p. 275.
[35] J.O. Park, C.H. Paik, Y.H. Huang, R.C. Alkire, J. Electrochem. Soc. 146 (1999) 517.
[36] R.G. Buchheit, R.P. Grant, P.F. Hlava, B. Mckenzie, G.L. Zender, J. Electrochem. Soc. 144 (1997) 2621.
[37] C.M. Liao, J.M. Olive, M. Gao, R.P. Wei, Corrosion 54 (1998) 451.
[38] Y. Liua, G.Z. Menga, Y.F. Chenga, Electrochim. Acta 54 (2009) 4155.
[39] C.J. Lin, R.G. Du, T. Nguyen, Corrosion 56 (2000) 41.
[40] K.A. Yasakau, M.L. Zheludkevich, S.V. Lamaka, M.G.S. Ferreira, Electrochim. Acta 52 (2007) 7231.
[41] R. Singh, J. Mater. Protec. 206 (2008) 286.